Int. J. Anal. Appl. (2024), 22:155

International Journal of Analysis and Applications

Nonlinear Steady-State VOC and Oxygen Modeling in Biofiltration

R. Vignesh Raju, S.G. Karpagavalli, R. Swaminathan*

PG & Research Department of Mathematics, Vidhyaa Giri College of Arts and Science, Affiliated to Alagappa University, Puduvayal - 630 108, India

**Corresponding author:* swaminathanmath@gmail.com

Abstract. This paper compares analytical solutions for steady-state volatile organic compounds (VOC) and oxygen concentrations in the context of bio-filtration modeling. Based on a set of nonlinear reaction/diffusion equations, this model consists of the following components:

- A nonlinear term from Monod kinetics and Andrew kinetics.
- A Monod kinetics, interactive model.
- An Andrews kinetics, interactive model.

The theoretical findings are helpful in the design of bio-filters. The ability of two independent strategies, the Akbar Ganji Method (AGM) and the Homotopy perturbation Method (HPM), to forecast steady-state concentrations is tested. The study investigates the advantages and disadvantages of both techniques, shedding insight into their practical usefulness in bio-filtration systems. The outcomes of this study lead to a better understanding of bio-filtration processes. They could influence the design.

1. Introduction

Bio-filtration is a commonly used environmental method that employs microorganisms to biodegrade pollutants such as VOCs in contaminated air or water streams. The efficacy of such systems is determined by the amounts of pollutants and oxygen, making it critical to understand and model their behavior precisely. To optimize the design and operating parameters, it is imperative to model the nonlinear steady-state behaviour of oxygen and VOCs in biofiltration systems. The intricate relationships and feedback mechanisms between substrate concentration, oxygen availability, and microbial activity are considered by nonlinear models. Gaining insight into these dynamics makes it possible to forecast how well biofilters will operate in different scenarios, which contributes to removing VOCs with the highest possible efficiency and dependability.

Received: Jul. 18, 2024.

2020 *Mathematics Subject Classification.* 35Q92.

Key words and phrases. bio-filters; volatile organic compounds; oxygen; mathematical modeling; Akbar Ganji method; homotopy perturbation method.

https://doi.org/10.28924/2291-8639-22-2024-155
ISSN: 2291-8639

This study aims to evaluate the efficacy and precision of the AGM and HPM techniques [3] in providing analytical solutions for the steady-state concentrations of oxygen and volatile organic compounds in bio-filtration systems. Analytical approaches are helpful because they provide insight into the system's behavior without requiring laborious numerical simulations. The work aims to advance knowledge of bio-filtration modeling by contrasting these two distinct analytical methodologies and offering insights into each approach's potential benefits and drawbacks. The findings of this study may enhance and optimize the efficacy of bio-filtration systems used in environmental remediation.

The Mixed-Solvent Removal Kinetics in a Biofilter for Waste Gas: Modeling and Experiments analysis [2]. Biofiltration-Based Modeling for Air Contamination Removal [4]. Comparing and Analyzing Biofilter Models [6]. Approximate Analytical Solutions [7] for Seepage Flow in Porous Media Using Fractional Derivatives. How to Address Boundary Value Issues Using the Homotopy Perturbation Method [9]. The Adomian Decomposition Method for Two-Point Boundary Value was applied by B. Jang [11]. Nonlinear Stochastic Simulation of Changes in a Nuclear Reactor—A Novel Approach by G. Adomian [13]. Solution of Parabolic Equations: Linear and Nonlinear using the Decomposition Method, by A. Saufyane and M. Boulmalf [14]. Sivasankari et al. [16] Analytical Expressions of Oxygen and VOC Concentrations in Steady-State Biofilteration Model using Adomian Decomposition Method

However, no analytical formulas for the steady-state concentrations of oxygen, VOC, and efficacy factor have been provided as of yet. This work aims to use the Homotopy Perturbation Method [18] and the Akbar Ganji Method [5] to determine the oxygen and volatile organic compound (VOC) content analytically for every parameter value and reaction process.

2. Mathematical formulation of the problem

A collection of mass balances within the biofilm makes up a steady-state biofilteration model. The following mass balance equations apply to the biofilm [16]:

$$D_1 \frac{d^2 m}{d\chi^2} = \frac{U}{V} \lambda(m, a) \tag{2.1}$$

$$D_2 \frac{d^2 a}{d\chi^2} = \frac{U}{V_1} \lambda(m, a) \tag{2.2}$$

With boundary conditions

$$m = \frac{m_h}{k} \ \ and \ \ a = \frac{m_{h_1}}{k_1} \ \ at \ \ \chi = 0 \tag{2.3}$$

$$\frac{dm}{d\chi} \ \ and \ \ \frac{da}{d\chi} \ \ at \ \ \chi = \beta \tag{2.4}$$

The symbols for biofilm density are U, V, V_1, D_1, D_2, where χ is the point in the biofilm where the concentration of VOC and oxygen is between m and a and is the effective diffusion coefficient of VOC and oxygen. These symbols also represent the cost per unit of oxygen used and the total

amount of biomass generated for every unit of VOC used. The growth rate $\lambda(m,a)$, for different reaction kinetics in biological systems is provided as follows:

Monod kinetics:

$$\lambda(m) = \frac{\lambda_m m}{L+m} \tag{2.5}$$

Andrews kinetics:

$$\lambda(m) = \frac{\lambda^* m}{L+m+\frac{m^2}{L_1}} \tag{2.6}$$

The interactive model provides a growth rate when the biodegradation rate is limited by oxygen. The following is the expression for equations (2.5) and (2.6) above:

From the interactive model, Monod kinetics.

$$\lambda(m,a) = \frac{\lambda_m m}{L+m}[\frac{a}{L_0+a}] \tag{2.7}$$

From Andrew kinetics, an interactive model

$$\lambda(m,a) = \frac{\lambda^* m}{L+m+\frac{m^2}{L_1}}[\frac{a}{L_0+a}] \tag{2.8}$$

A numerical solution for the model is obtained by transforming these equations into a dimensionless form using dimensionless variables and groups. To generate those above non-linear partial differential equations (2.1) and (2.2), the dimensionless form of the subsequent dimensionless parameters is defined:

$$M = \frac{mk}{m_h},\ A = \frac{ak_1}{a_h 1},\ \chi = \frac{x}{\beta},\ \pi^2 = \frac{U\lambda_m \beta^2}{LD_1 V},\ \theta = \frac{D_1 V a_h a_h 1}{D_2 V_1 k k_1},\ P = \frac{a_h}{L_1 k},\ Q = \frac{a_h}{L_2 k}\ R = \frac{L_0 k_1}{a_h 1} \tag{2.9}$$

In the biolayer, χ represents the dimensionless position, and M and A indicate the dimensionless concentration of oxygen and VOC, respectively. The Thiele modulus is denoted by ϕ, while θ, P, Q, and R are dimensionless constants. It is possible to swap Equations (2.1) & (2.2) into Equation (2.9) to obtain the dimensionless non-linear Equation for Monod kinetics that follows:

$$\frac{d^2 M(\chi)}{d\chi^2} = \phi^2 \left[\frac{M(\chi)}{1+PM(\chi)}\right] \tag{2.10}$$

$$\frac{d^2 A(\chi)}{d\chi^2} = \phi^2 \theta \left[\frac{M(\chi)}{1+PM(\chi)}\right] \tag{2.11}$$

Using (2.9), we may obtain the dimensionless Equation for Andrews kinetics, which is present in the nonlinear Equations (2.1) and (2.2).

$$\frac{d^2 M(\chi)}{d\chi^2} = \phi^2 \left[\frac{M(\chi)}{1+PM(\chi)+PQM(\chi)^2}\right] \tag{2.12}$$

$$\frac{d^2A(\chi)}{d\chi^2} = \phi^2\theta\left[\frac{M(\chi)}{1+PM(\chi)+PQM(\chi)^2}\right] \tag{2.13}$$

Through the use of Equation (2.9), the interactive model of Monod kinetics dimensionless nonlinear equation becomes

$$\frac{d^2M(\chi)}{d\chi^2} = \phi^2\left[\frac{M(\chi)}{1+PM(\chi)}\right]\left[\frac{A(\chi)}{R+A(\chi)}\right] \tag{2.14}$$

$$\frac{d^2A(\chi)}{d\chi^2} = \phi^2\theta\left[\frac{M(\chi)}{1+PM(\chi)}\right]\left[\frac{A(\chi)}{R+A(\chi)}\right] \tag{2.15}$$

A dimensionless nonlinear equation can be obtained by combining the dimensionless nonlinear equations (2.1) & (2.2) of the Andrews kinetics interactive model.

$$\frac{d^2M(\chi)}{d\chi^2} = \phi^2\left[\frac{M(\chi)}{1+PM(\chi)+PQM(\chi)^2}\right]\left[\frac{A(\chi)}{R+A(\chi)}\right] \tag{2.16}$$

$$\frac{d^2A(\chi)}{d\chi^2} = \phi^2\theta\left[\frac{M(\chi)}{1+PM(\chi)+PQM(\chi)^2}\right]\left[\frac{A(\chi)}{R+A(\chi)}\right] \tag{2.17}$$

The boundary condition can now be expressed as follows in dimensionless form:

$$M = 1 \ \textit{and} \ A = 1 \ \textit{at} \ \chi = 0 \tag{2.18}$$

$$\frac{dM}{d\chi} = 0 \ \textit{and} \ \frac{dA}{d\chi} \ \textit{at} \ \chi = 1 \tag{2.19}$$

3. Approximate analytical expressions for current and concentrations

Approximate analytical methods refer to mathematical techniques for solving complex problems where exact solutions are difficult or impossible. These methods involve approximating and simplifying the situation while still aiming to provide useful and accurate results. Some standard approximate analytical methods are Variation Iterational Method [1], Homotopy Perturbation Method [8], Adomian Decomposition Method [7], Differential Transform Method [21], Akbar Ganji Method [15].

3.1. **Approximate analytical responses of the concentrations were obtained using the Akbar Ganji Method (AGM).** The nonlinear differential equations controlling this system are solved in this paper using the Akbar-Ganji technique developed by mathematicians Akbar and Ganji [10]. We can solve the nonlinear equations quickly using this method, which removes the requirement for challenging mathematical processes. This method is appropriate and accessible for solving nonlinear differential equations.

Although numerical approaches can yield accurate and economical approximate solutions for nonlinear systems, they have notable limitations that should be considered. Significant difficulties can arise when adjusting parameters to match the numerical data, and numerical stability is needed to obtain numerical solutions. Because analytical solutions offer a more comprehensive grasp of how model parameters affect analysis, researchers tend to favour them.

The concentrations yield the approximate analytical expressions that follow, as shown in Appendix A when the AGM technique is applied [12]: The VOC concentration for Monod kinetics can be found by applying the following method to the solutions of Equations (2.10) & (2.11):

$$M(\chi) = cosh(m_1\chi) - \frac{sinh(m_1)sinh(m_1\chi)}{cosh(m_1)} \tag{3.1}$$

$$where \;\; m_1 = \frac{\phi}{\sqrt{P+1}} \tag{3.2}$$

$$A(\chi) = cosh(n_1\chi) - \frac{sinh(n_1)sinh(n_1\chi)}{cosh(n_1)} \tag{3.3}$$

$$where \;\; n_1 = \frac{\sqrt{(P+Q)\theta\phi}}{P+1} \tag{3.4}$$

The VOC concentration can be determined as follows: By using Andrews kinetics and solving Equations (2.12) and (2.13),

$$M(\chi) = cosh(m_2\chi) - \frac{sinh(m_2)sinh(m_2\chi)}{cosh(m_2)} \tag{3.5}$$

$$where \;\; m_2 = \frac{\phi}{\sqrt{PQ+P+1}} \tag{3.6}$$

$$A(\chi) = cosh(n_2\chi) - \frac{sinh(n_2)sinh(n_2\chi)}{cosh(n_2)} \tag{3.7}$$

$$where \;\; n_2 = \frac{\sqrt{(PQ+P+1)\theta\phi}}{PQ+P+1} \tag{3.8}$$

It is possible to determine the VOC concentration in the interactive Monod kinetics model as follows by solving Equations (2.14) and (2.15):

$$M(\chi) = cosh(m_3\chi) - \frac{sinh(m_3)sinh(m_3\chi)}{cosh(m_3)} \tag{3.9}$$

$$where \;\; m_3 = \frac{\phi}{\sqrt{PR+P+R+1}} \tag{3.10}$$

$$A(\chi) = cosh(n_3\chi) - \frac{sinh(n_3)sinh(n_3\chi)}{cosh(n_3)} \tag{3.11}$$

$$where \;\; n_3 = \frac{\sqrt{(PR+P+R+1)\theta\phi}}{PR+P+R+1} \tag{3.12}$$

Through the following procedure, the VOC concentration in the interactive model of Andrews kinetics can be determined by solving Equations (2.16) and (2.17).

$$M(\chi) = cosh(m_4\chi) - \frac{sinh(m_4)sinh(m_4\chi)}{cosh(m_4)} \tag{3.13}$$

$$where\ \ m_4 = \frac{\phi}{\sqrt{QPR + QP + PR + P + R + 1}} \tag{3.14}$$

$$A(\chi) = cosh(n_4\chi) - \frac{sinh(n_4)sinh(n_4\chi)}{cosh(n_4)} \tag{3.15}$$

$$where\ \ n_4 = \frac{\sqrt{(QPR + QP + PR + P + R + 1)\theta\phi}}{QPR + QP + PR + P + R + 1} \tag{3.16}$$

3.2. **Approximate analytical responses of the concentrations were obtained using the Homotopy Perturbation Method (HPM).** In many branches of science and engineering, non-linear phenomena are fundamentally important. Solving most real-life problem models remains a challenging task. As a result, rough analytical solutions like the Homotopy perturbation method (HPM) were brought forth. For non-linear equations, the HPM is the most practical and efficient approach [17]. Assuming a small parameter is the foundation of the perturbation approach. Many authors in the physical sciences and engineering have recently turned to the HPM for solutions to non-linear problems. Some non-linear problems in the physical sciences can be solved by combining classical perturbation techniques with topology's homotopy [20]. The HPM is exceptional because it is efficient, accurate, and applicable. The HPM only requires a small number of iterations in the embedding parameters to find an asymptotic solution. The approximate analytical formulas of concentrations that follow (Appendix B) are generated using the HPM approach [19]: By solving the Equation (2.10) & (2.11), the VOC concentration for Monod kinetics can be determined as follows:

$$M(\chi) = \frac{(\chi^2 - 2\chi)\phi^2 + 2P + 2}{2P + 2} \tag{3.17}$$

$$A(\chi) = \frac{\chi\theta(\chi - 2)\phi^2 + 2P + 2}{2P + 2} \tag{3.18}$$

Andrews kinetics VOC concentration may be found by solving Equations (2.12) and (2.13).

$$M(\chi) = \frac{(2Q + 2)P + 2 + (\chi^2 - 2\chi)\phi^2}{2 + (2Q + 2)P} \tag{3.19}$$

$$A(\chi) = \frac{(2Q + 2)P + 2 + (\chi^2 - 2\chi)\phi^2\theta}{2 + (2Q + 2)P} \tag{3.20}$$

Solving Equations (2.14) and (2.15) obtains the VOC concentration for the interactive model of Monod kinetics.

$$M(\chi) = \frac{(2R + 2)P + 2R + 2 + (\chi^2 - 2\chi)\phi^2}{2(P + 1)(R + 1)} \tag{3.21}$$

$$A(\chi) = \frac{(2R + 2)P + 2R + 2 + (\chi^2 - 2\chi)\phi^2\theta}{2(P + 1)(R + 1)} \tag{3.22}$$

Equations (2.16) and (2.17) can be solved to determine the VOC concentration for the interactive Andrews kinetics model.

$$M(\chi) = \frac{2(Q+1)(R+1)P + 2R + 2 + (\chi^2 - 2\chi)\phi^2}{2(R+1)(1+(Q+1)P} \tag{3.23}$$

$$A(\chi) = \frac{2(Q+1)(R+1)P + 2R + 2 + (\chi^2 - 2\chi)\phi^2\theta}{2(R+1)(1+(Q+1)P} \tag{3.24}$$

4. Effectiveness factor

The natural reaction rate is divided by the reaction rate when the entire biofilm is exposed to the concentration at the gas/biofilm interface. This ratio is known as the efficacy factor. These are some of the different kinetics efficacy factors:

Monod Kinetics:

$$\eta = \frac{-(1+P)}{\phi^2}\left(\frac{dM}{d\chi}\right)_{\chi=0} = \frac{\sqrt{1+P}sinh\left(\frac{\phi}{\sqrt{1+P}}\right)}{\phi cosh\left(\frac{\phi}{\sqrt{1+P}}\right)} \tag{4.1}$$

Andrews kinetics:

$$\eta = \frac{-(1+P+PQ)}{\phi^2}\left(\frac{dM}{d\chi}\right)_{\chi=0} = \frac{\sqrt{PQ+P+1}sinh\left(\frac{\phi}{\sqrt{PQ+P+1}}\right)}{\phi^2 cosh\left(\frac{\phi}{\sqrt{PQ+P+1}}\right)} \tag{4.2}$$

From Monod kinetics, an interactive model

$$\eta = \frac{-(1+P)(Q+1)}{\phi^2}\left(\frac{dM}{d\chi}\right)_{\chi=0} = \frac{(1+P)(Q+1)sinh\left(\frac{\phi}{\sqrt{(1+P)(Q+1}}\right)}{\sqrt{(1+P)(Q+1)}\phi cosh\left(\frac{\phi}{\sqrt{(1+P)(N+1}}\right)} \tag{4.3}$$

From Andrew kinetics, an interactive model

$$\eta = -\frac{-(1+P+PQ)(R+1)}{\phi^2}\left(\frac{dM}{d\chi}\right)_{\chi=0} = \frac{(QP+P+1)(R+1)sinh\left(\frac{\phi}{\sqrt{(R+1)(QP+P+1)}}\right)}{\sqrt{(R+1)(QP+P+1)}\phi cosh\left(\frac{\phi}{(R+1)(QP+P+1}\right)} \tag{4.4}$$

5. Numerical Simulation

By using numerical techniques, Equations (2.10)–(2.17) in their dimensionless version, which match the boundary conditions (2.18) and (2.19), were resolved. To solve differential equations' initial boundary value problems, we employed pdex4, a function available in MATLAB. The numerical solution to Equations (2.10) and (2.11) can be found using the Matlab program provided in Appendix C. In Figures 1–16, the numerical solution is displayed and contrasted with our analytical findings. A good agreement is seen for a range of Thiele modulus values and potentially low reaction/diffusion parameter values.

6. Result and Discussion

For all parameter values, the updated analytical formulas for the VOC concentration in the kinetics of Monod, Andrews, Interactive Monod, and Interactive Andrews are represented by equations (2.10)–(2.17). The concentrations of volatile organic compounds (VOC), denoted as $M(\chi)$ and oxygen, denoted as $A(\chi)$ are influenced by various parameters including ϕ, P, Q, R and θ Adjusting these parameters can lead to changes in the concentrations of $M(\chi)$ and $A(\chi)$ as follows:

6.1. **The Thiele Modulus.** The Thiele modulus is a crucial indicator that contrasts the biodegradation rate against the diffusion rate. Two conditions cause variations in the concentration profiles:

- Enzyme kinetics control indicates that the total amount of active enzyme determines the overall reaction rate when the Thiele modulus is small.
- Diffusion control takes over when the Thiele modulus is high. This condition occurs when the diffusion coefficient or reaction rate constant is low or when there is vigorous catalytic activity and increased membrane thickness.

6.2. **Monod Kinetics.** Monod kinetics VOC concentration in the biofilm is represented by equation (2.10 & 2.11). Equation (3.1) & (3.17), the dimensionless concentration $M(\chi)$ against dimensionless distance (χ) in Figures 1 & 2 is applied to a range of values of the Thiele modulus (ϕ) and the dimensionless parameter (P). As the value of ϕ or the thickness of the biofilter diminishes, these figures show that the concentration of VOCs at $\chi = 1$ increases. In addition, the concentration is constant for all values of $M(\chi)$ when $\phi \leq 0.1$ and all the values of P. For a range of values of the dimensionless parameters, θ, P, and the Thiele modulus ϕ, the dimensionless concentration plot, denoted by $A(\chi)$ (3.3) & (3.18), is displayed in Figures 3 & 4. These figures unequivocally demonstrate that the oxygen content decreases as θ increases.

6.3. **Andrew Kinetics.** The concentration of volatile organic compounds under Andrews-type kinetics is defined by equation (2.12 & 2.13). Equations (3.5) & (3.19), For various combinations of dimensionless parameters, the dimensionless concentration $M(\chi)$ as a function of dimensionless distance χ is represented in Figures 5 & 6. These graphs demonstrate that when P, Q, and ϕ rise, the VOC concentration decreases. The dimensionless concentration $A(\chi)$, (3.7) & (3.20) is shown in Figures 7 & 8 for different combinations of the dimensionless parameters θ, P, Q, and *phi*.

6.4. **Interactive Monod Kinetics.** The Interactive model's VOC concentration, obtained using Monod kinetics, is shown in equation (2.14 & 2.15). Equations (3.9) & (3.21), used for different parameter configurations, shows the dimensionless concentration $M(\chi)$ vs dimensionless distance χ in Figures 9 & 10. These graphs show that when $\theta \leq 10$, the VOC concentration is homogeneous. Furthermore, when θ grows, $A(\chi)$ decreases. Figures 11 & 12 display the dimensionless concentration $A(\chi)$ for different combinations of dimensionless parameters θ, P, R, and ϕ. These figures suggest that when $\phi \leq 0.5$ for all parameter sets, $M(\chi) = 1$.

6.5. **Interactive Andrew Kinetics.** The VOC concentration in the Interactive model under Andrews kinetics is represented by equation (2.16 & 2.17). For various values of the Thiele modulus (ϕ, P, Q, R, and θ), Figures 13 & 14 plot the dimensionless concentration $M(\chi)$ against the dimensionless distance (χ) using Equation (3.13) & (3.23). The dimensionless concentration $A(\chi)$ for various combinations of dimensionless parameters is displayed in Figures 15 & 16. These numbers show that when the bio-filter thickness ϕ drops, the VOC concentration $M(\chi)$ stays constant.

6.6. **Effectiveness Factor.** Equations (4.1)–(4.4) were used to compute the effectiveness factor η, displayed against the Thiele modulus ϕ in Figures 17 and 18. These numbers clearly show that for all methods, when $\phi \leq 0.2$, the efficacy factor η hits 1.

7. Conclusion

In conclusion, this study has looked into how to improve indoor air quality by biofiltration modeling using asymptotic approaches. We have created new analytical formulas for oxygen and VOC concentrations by examining various kinetic models, including Monod, Andrews, Interactive Monod, and Interactive Andrews. These formulas provide essential information about how several parameters affect the efficiency of biofilters, including the Thiele modulus phi, catalytic activity, membrane thickness, and reaction rate constants K. We found that a small Thiele modulus (ϕ) denotes a dominance of enzyme kinetics, in which the availability of active enzymes predominantly controls the reaction rate. Conversely, greater (ϕ) values indicate diffusion control, which is impacted by elements like membrane thickness and catalytic activity. The effectiveness factor (η) research revealed that when $\phi \leq 0.2$, it stays high $(\eta = 1)$, showing successful removal of contaminants across different biofiltration processes. Changes in ϕ, P, Q, R and θ parameters considerably affected the concentration profiles of oxygen and VOCs, highlighting the complex link between pollutant removal effectiveness and biofilter configuration.

The mathematical modeling of nonlinear reaction/diffusion at steady-state concentrations of oxygen and volatile organic compounds (VOCs) in bio-filtration has given us a critical new understanding of the complex dynamics of these systems. We have proven that these approximate analytical methods help solve the governing equations of the bio-filtration process by applying mathematical solid techniques such as the AGM (Akbar Ganji Method) and HPM (Homotopy Perturbation Method).

Our results emphasize how crucial it is to consider diffusion effects and nonlinearities when simulating the breakdown of volatile organic compounds and the distribution of oxygen within biofilters. The created models help design and manage effective VOC removal processes by providing a way to forecast and maximize the performance of bio-filtration systems. Overall, our research establishes a platform for future investigation and development in this vital area of environmental engineering and emphasizes the value of mathematical modeling in deepening our understanding of bio-filtration processes.

χ	$\phi = 0.1$					$\phi = 0.3$					$\phi = 0.5$				
	AGM	**HPM**	**NUM**	**Error % using (3.1)**	**Error % using (3.17)**	**AGM**	**HPM**	**NUM**	**Error % using (3.1)**	**Error % using (3.17)**	**AGM**	**HPM**	**NUM**	**Error % using (3.1)**	**Error % using (3.17)**
0	1	1	1	0	0	1	1	1	0	0	1	1	1	0	0
0.2	0.9982	0.9982	0.9982	0	0	0.9843	0.9837	0.9843	0	0.0609	0.9584	0.9546	0.9584	0	0.3964
0.4	0.9968	0.9968	0.9968	0	0	0.9721	0.971	0.9721	0	0.1131	0.9265	0.9195	0.9261	0.0431	0.7126
0.6	0.9958	0.9958	0.9958	0	0	0.9636	0.962	0.9636	0	0.1660	0.9042	0.8945	0.9029	0.1439	0.9303
0.8	0.9952	0.9952	0.9952	0	0	0.9585	0.9567	0.9585	0	0.1877	0.891	0.8797	0.8885	0.2813	0.9904
1	0.995	0.995	0.995	0	0	0.957	0.955	0.957	0	0.2089	0.8869	0.8751	0.8829	0.4530	0.8834
	Average Error %			**0**	**0**				**0**	**0.1228**				**0.1535**	**0.6522**

TABLE 1. Comparison of analytical solutions, with different ϕ values, and fixed parameter values P from numerical simulation

χ	$\theta = 10$					$\theta = 50$					$\theta = 100$				
	AGM	**HPM**	**NUM**	**Error % using (3.3)**	**Error % using (3.18)**	**AGM**	**HPM**	**NUM**	**Error % using (3.3)**	**Error % using (3.18)**	**AGM**	**HPM**	**NUM**	**Error % using (3.3)**	**Error % using (3.18)**
0	1	1	1	0	0	1	1	1	0	0	1	1	1	0	0
0.2	0.9818	0.9818	0.9818	0	0	0.8657	0.8184	0.8184	5.7795	0	0.8657	0.8184	0.8184	5.7795	0
0.4	0.9677	0.9677	0.9677	0	0	0.7668	0.6775	0.6775	13.1808	0	0.7668	0.6775	0.6775	13.1808	0
0.6	0.9577	0.9577	0.9577	0	0	0.6992	0.5773	0.5773	21.1155	0	0.6992	0.5773	0.5773	21.1155	0
0.8	0.9518	0.9518	0.9518	0	0	0.6603	0.5177	0.5177	27.5449	0	0.6603	0.5177	0.5177	27.5449	0
1	0.9499	0.9499	0.9499	0	0	0.6483	0.4987	0.4987	29.9979	0	0.6483	0.4987	0.4987	29.9979	0
	Average Error %			**0**	**0**				**16.2698**	**0**				**16.2698**	**0**

TABLE 2. Comparison of analytical solutions, with different θ values, and fixed parameter values of P and ϕ from numerical simulation

χ	$\phi = 0.1$					$\phi = 0.3$					$\phi = 0.5$				
	AGM	**HPM**	**NUM**	**Error % using (3.5)**	**Error % using (3.19)**	**AGM**	**HPM**	**NUM**	**Error % using (3.5)**	**Error % using (3.19)**	**AGM**	**HPM**	**NUM**	**Error % using (3.5)**	**Error % using (3.19)**
0	1	1	1	0	0	1	1	1	0	0	1	1	1	0	0
0.2	0.99	0.99	0.99	0	0	0.9843	0.9843	0.9843	0	0	0.9587	0.9551	0.9584	0	0
0.4	0.99	0.99	0.99	0	0	0.9721	0.9721	0.9721	0	0	0.9272	0.9202	0.9261	0	0
0.6	0.99	0.99	0.99	0	0	0.9636	0.9636	0.9636	0	0	0.9049	0.8955	0.9029	0	0
0.8	0.99	0.99	0.99	0	0	0.9585	0.9585	0.9585	0	0	0.8919	0.8808	0.8886	0	0
1	0	0	0	0	0	0.957	0.957	0.957	0	0	0.8878	0.8762	0.883	0	0
	Average Error %			**0**	**0**				**0**	**0**				**0**	**0**

TABLE 3. Comparison of analytical solutions, with different ϕ values, and fixed parameter values P and Q from numerical simulation

χ	$\theta = 10$					$\theta = 50$					$\theta = 100$				
	AGM	**HPM**	**NUM**	**Error % using (3.7)**	**Error % \using (3.20)**	**AGM**	**HPM**	**NUM**	**Error % using (3.7)**	**Error % using (3.20)**	**AGM**	**HPM**	**NUM**	**Error % using (3.7)**	**Error % using (3.20)**
0	1	1	1	0	0	1	1	1	0	0	1	1	1	0	0
0.2	0.9825	0.9819	0.9818	0.07129	0.0101	0.923	0.9094	0.9092	1.5178	0.0219	0.8657	0.8189	0.8184	5.7795	0.0610
0.4	0.969	0.9679	0.9677	0.1343	0.0206	0.8649	0.8395	0.8387	3.1238	0.0953	0.6668	0.6789	0.6775	1.5793	0.2066
0.6	0.9594	0.958	0.9577	0.1775	0.0313	0.8044	0.7899	0.7886	2.0035	0.1648	0.5992	0.5798	0.5773	3.7935	0.4330
0.8	0.9538	0.9521	0.9518	0.2101	0.0315	0.7508	0.7606	0.7589	1.0673	0.2240	0.5003	0.5212	0.5177	3.3610	0.6760
1	0.952	0.9503	0.9499	0.2210	0.0421	0.7534	0.7515	0.7494	0.5337	0.2802	0.5083	0.503	0.4987	1.9250	0.8622
	Average Error %			**0.1357**	**0.0226**				**1.0186**	**0.1310**				**1.0929**	**0.3731**

TABLE 4. Comparison of analytical solutions, with different θ values, and fixed parameter values of P, Q and ϕ from numerical simulation

χ	$\phi = 0.1$					$\phi = 0.3$					$\phi = 0.5$				
	AGM	**HPM**	**NUM**	**Error % using (3.9)**	**Error % using (3.21)**	**AGM**	**HPM**	**NUM**	**Error % using (3.9)**	**Error % using (3.21)**	**AGM**	**HPM**	**NUM**	**Error % using (3.9)**	**Error % using (3.21)**
0	1	1	1	0	0	1	1	1	0	0	1	1	1	0	0
0.2	0.9991	0.9991	0.9991	0	0	0.9842	0.9837	0.9918	0.7662	0.8166	0.9584	0.9547	0.9783	2.0341	2.4123
0.4	0.9984	0.9984	0.9984	0	0	0.972	0.971	0.9854	1.3598	1.4613	0.9566	0.9596	0.9616	0.5199	0.2079
0.6	0.9979	0.9979	0.9979	0	0	0.9634	0.9621	0.9808	1.7740	1.9066	0.9343	0.9346	0.9498	1.6319	1.600
0.8	0.9976	0.9976	0.9976	0	0	0.9583	0.9567	0.9779	2.0042	2.1679	0.9011	0.9098	0.943	4.4432	3.5206
1	0.9975	0.9975	0.9975	0	0	0.9567	0.9551	0.9769	2.0677	2.2315	0.917	0.9152	0.941	2.5504	2.7417
	Average Error %			**0**	**0**				**1.3287**	**1.4306**				**1.8632**	**1.7471**

TABLE 5. Comparison of analytical solutions, with different ϕ values, and fixed parameter values of P, R and θ from numerical simulation

χ	$\theta = 10$					$\theta = 50$					$\theta = 100$				
	AGM	**HPM**	**NUM**	**Error % using (3.11)**	**Error % using (3.22)**	**AGM**	**HPM**	**NUM**	**Error % using (3.11)**	**Error % using (3.22)**	**AGM**	**HPM**	**NUM**	**Error % using (3.11)**	**Error % using (3.22)**
0	1	1	1	0	0	1	1	1	0	0	1	1	1	0	0
0.2	0.9819	0.9819	0.9909	0	0.9082	0.9231	0.9094	0.9524	3.0764	4.5149	0.8658	0.8187	0.8993	3.7251	8.9625
0.4	0.9678	0.9678	0.9839	0	1.6363	0.865	0.8391	0.9149	5.4541	8.2850	0.7669	0.6782	0.82	6.4756	17.2926
0.6	0.9578	0.9578	0.9789	0	2.1554	0.8325	0.7892	0.8875	6.1971	11.0760	0.6994	0.5784	0.7632	8.3595	24.2138
0.8	0.9519	0.9519	0.976	0	2.4692	0.8009	0.7597	0.8706	8.0059	12.7383	0.6605	0.5194	0.7296	9.4709	28.8103
1	0.9501	0.9501	0.9751	0	2.5638	0.7936	0.7505	0.8642	8.1694	13.1566	0.6485	0.501	0.7195	9.8679	30.3683
	Average Error %			**0**	**1.6221**				**5.1505**	**8.2951**				**6.3165**	**18.2746**

TABLE 6. Comparison of analytical solutions, with different θ values, and fixed parameter values of P, R and ϕ from numerical simulation

χ	$\phi = 0.1$					$\phi = 0.3$					$\phi = 0.5$				
	AGM	**HPM**	**NUM**	**Error % using (3.13)**	**Error % using (3.23)**	**AGM**	**HPM**	**NUM**	**Error % using (3.13)**	**Error % using (3.23)**	**AGM**	**HPM**	**NUM**	**Error % using (3.13)**	**Error % using (3.23)**
0	1	1	1	0	0	1	1	1	0	0	1	1	1	0	0
0.2	0.9982	0.9982	0.9982	0	0	0.9843	0.9843	0.9837	0.0609	0.0609	0.9584	0.9547	0.962	0.3742	0.7588
0.4	0.9968	0.9968	0.9968	0	0	0.9721	0.9721	0.971	0.1132	0.1132	0.9266	0.9196	0.9327	0.6540	1.4045
0.6	0.9958	0.9958	0.9958	0	0	0.9636	0.9636	0.9621	0.1559	0.1559	0.9043	0.8946	0.9119	0.8334	1.8971
0.8	0.9952	0.9952	0.9952	0	0	0.9585	0.9585	0.9567	0.1881	0.1881	0.8911	0.8799	0.8993	0.9118	2.1572
1	0.9954	0.9954	0.9954	0	0	0.957	0.957	0.9551	0.1989	0.1989	0.887	0.8753	0.8951	0.9049	2.2120
	Average Error %			**0**	**0**				**0.1195**	**0.1195**				**0.6130**	**1.4049**

TABLE 7. Comparison of analytical solutions, with different ϕ values, and fixed parameter values of P, Q, R and θ from numerical simulation

χ	$\theta = 10$					$\theta = 50$					$\theta = 100$				
	AGM	**HPM**	**NUM**	**Error % using (3.15)**	**Error % using (3.24)**	**AGM**	**HPM**	**NUM**	**Error % using (3.15)**	**Error % using (3.24)**	**AGM**	**HPM**	**NUM**	**Error % using (3.15)**	**Error % using (3.24)**
0	1	1	1	0	0	1	1	1	0	0	1	1	1	0	0
0.2	0.9825	0.9819	0.982	0.0509	0.0101	0.9231	0.9092	0.9092	1.5288	0	0.8158	0.8184	0.8184	0.3176	0
0.4	0.969	0.9678	0.9682	0.0826	0.0413	0.835	0.8387	0.8387	0.4411	0	0.7069	0.6775	0.6775	4.3394	0
0.6	0.9595	0.9578	0.9583	0.1252	0.0521	0.8045	0.7887	0.7887	2.0032	0	0.6094	0.5773	0.5773	5.5603	0
0.8	0.9538	0.9519	0.9526	0.1259	0.0734	0.7609	0.7589	0.7589	0.2635	0	0.5005	0.5178	0.5178	3.3410	0
1	0.9521	0.9501	0.9509	0.1261	0.0841	0.7936	0.7494	0.7494	5.8980	0	0.5085	0.4989	0.4989	1.9242	0
	Average Error %			**0.0851**	**0.0435**				**1.5420**	**0**				**1.3608**	**0**

TABLE 8. Comparison of analytical solutions, with different θ values, and fixed parameter values of P, Q, R and ϕ from numerical simulation

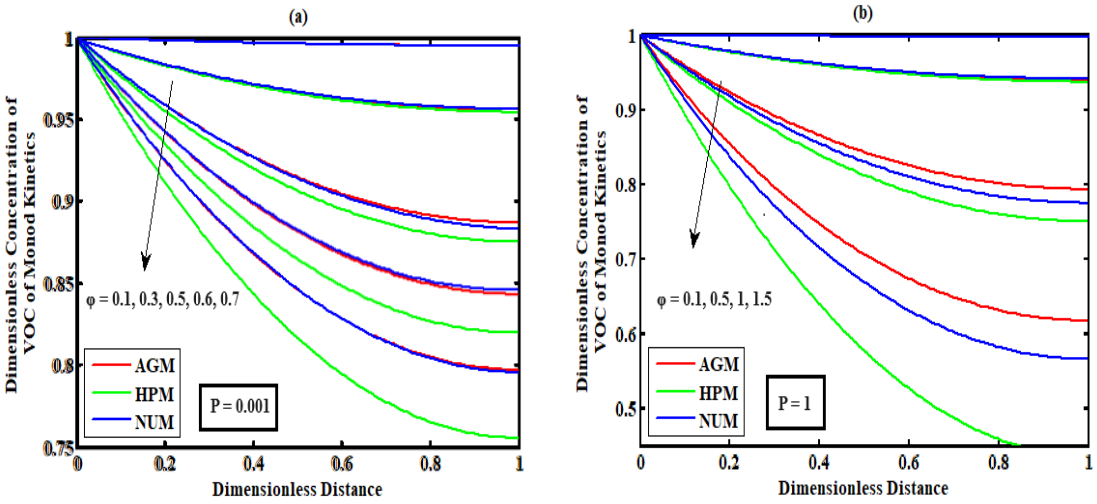

FIGURE 1. Plotting the dimensionless concentration $M(\chi)$ against the dimensionless distance χ for different Thiele moduli ϕ and P values using equations (3.1) and (3.17)

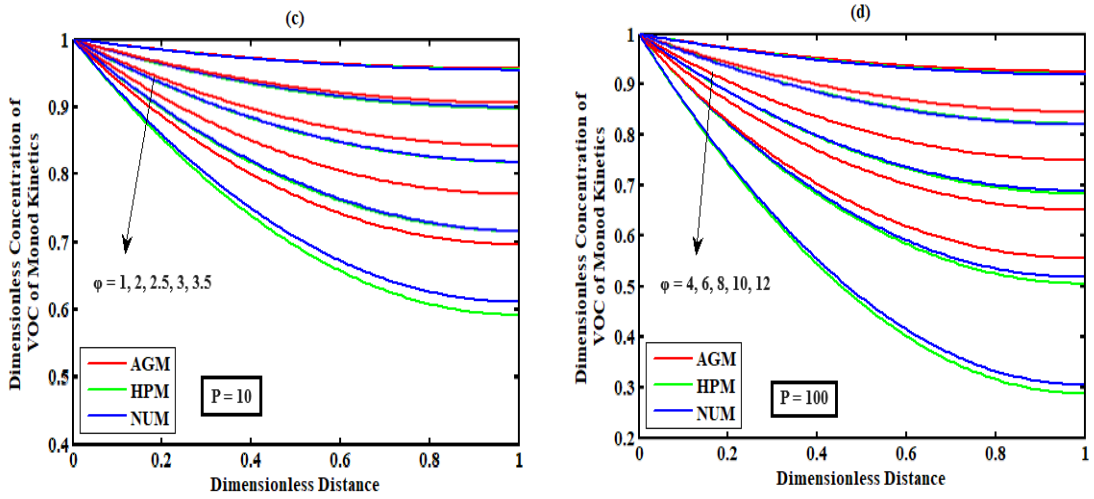

FIGURE 2. Plotting the dimensionless concentration $M(\chi)$ against the dimensionless distance χ for different Thiele moduli ϕ and P values using equations (3.1) and (3.17)

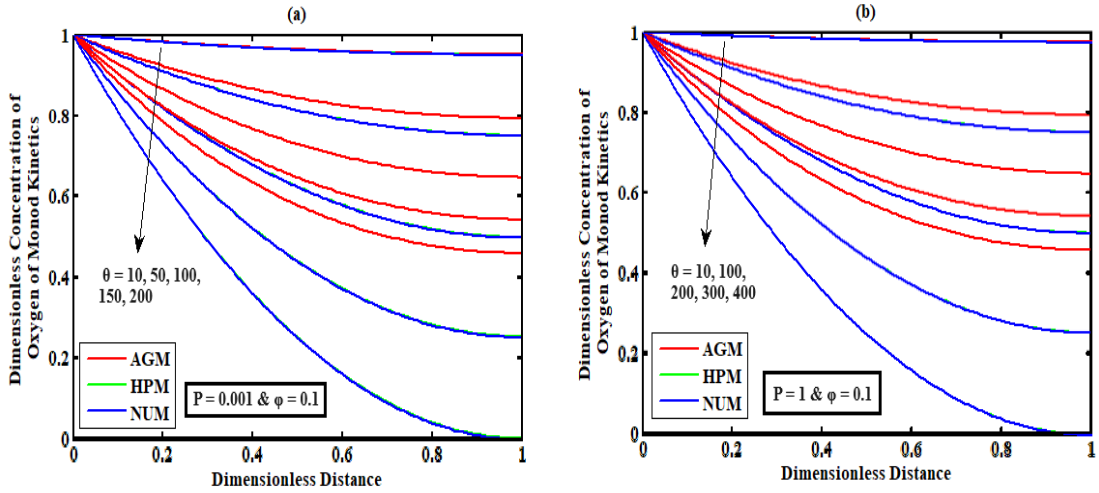

FIGURE 3. Plotting the dimensionless concentration $A(\chi)$ against the dimensionless distance χ for different Thiele moduli θ, P & ϕ values using equations (3.3) and (3.18)

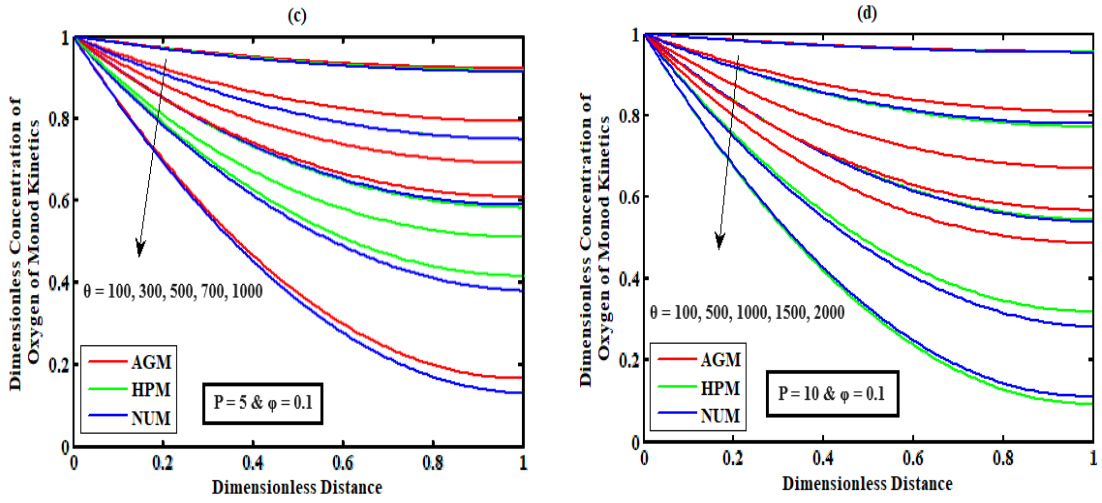

FIGURE 4. Plotting the dimensionless concentration $A(\chi)$ against the dimensionless distance χ for different Thiele moduli θ, P & ϕ values using equations (3.3) and (3.18)

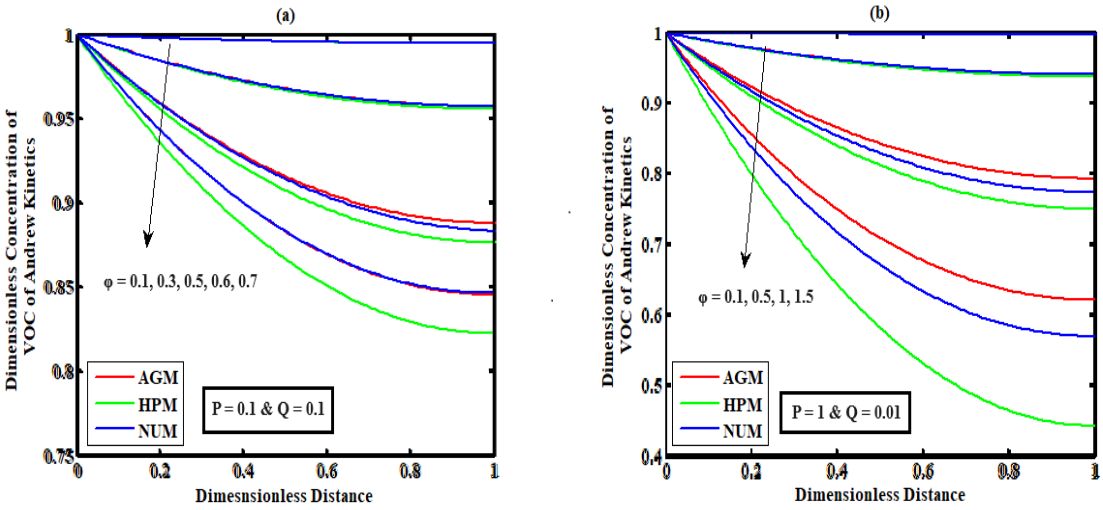

FIGURE 5. Plotting the dimensionless concentration $M(\chi)$ against the dimensionless distance χ for different Thiele moduli ϕ, P and Q values using equations (3.5) and (3.19)

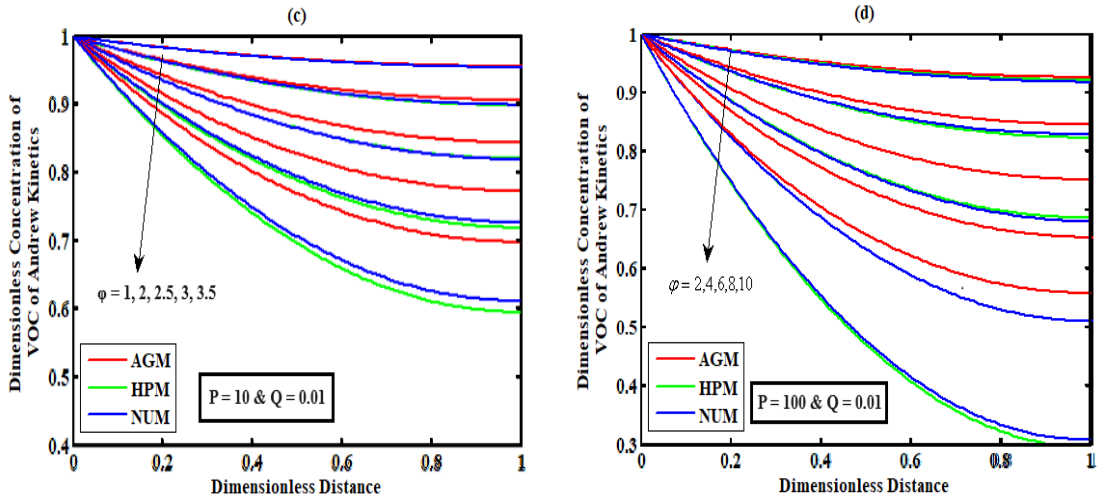

FIGURE 6. Plotting the dimensionless concentration $M(\chi)$ against the dimensionless distance χ for different Thiele moduli ϕ, P and Q values using equations (3.5) and (3.19)

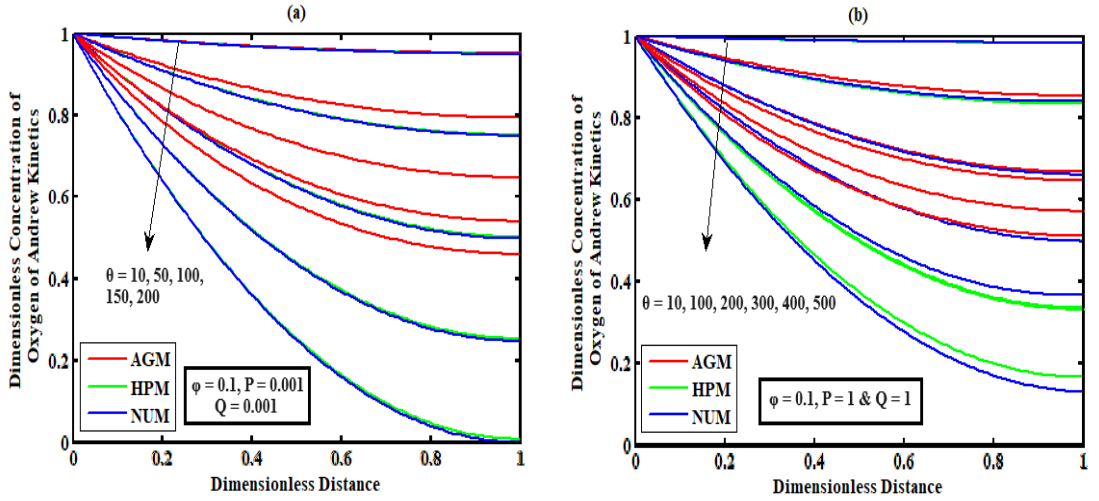

FIGURE 7. Plotting the dimensionless concentration $A(\chi)$ against the dimensionless distance χ for different Thiele moduli ϕ, P, Q & θ values using equations (3.7) and (3.20)

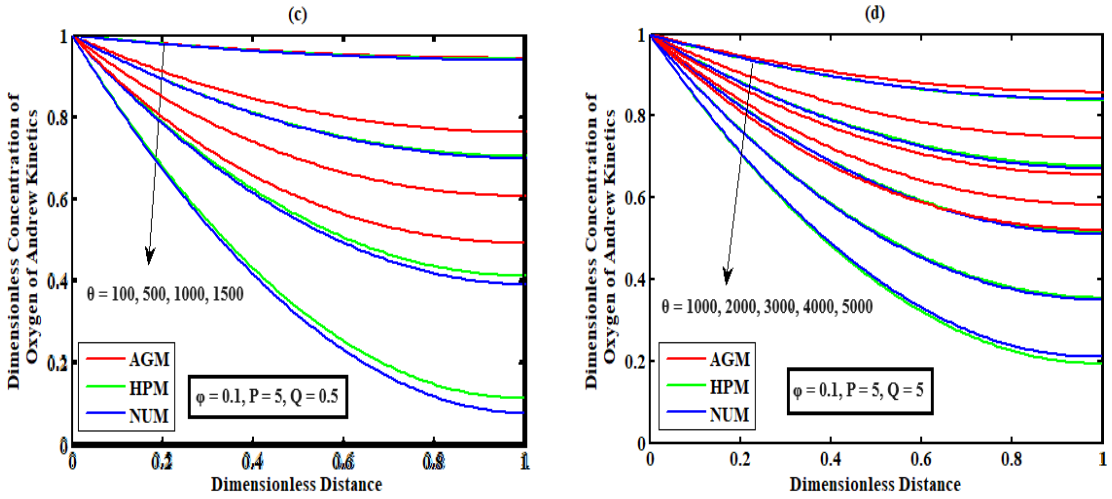

FIGURE 8. Plotting the dimensionless concentration $A(\chi)$ against the dimensionless distance χ for different Thiele moduli ϕ, P, Q & θ values using equations (3.7) and (3.20)

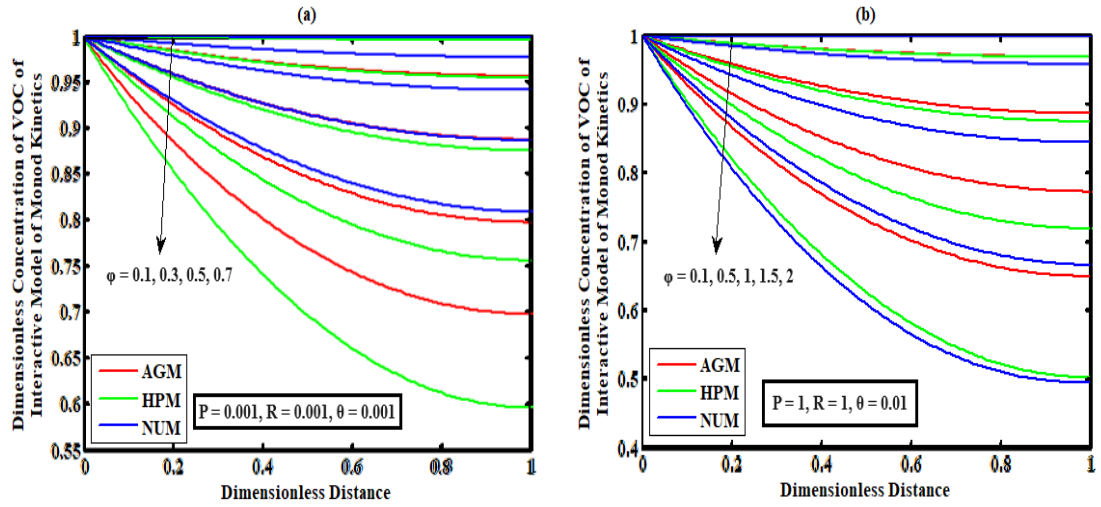

FIGURE 9. Plotting the dimensionless concentration $M(\chi)$ against the dimensionless distance χ for different Thiele moduli ϕ, P, R & θ values using equations (3.9) and (3.21)

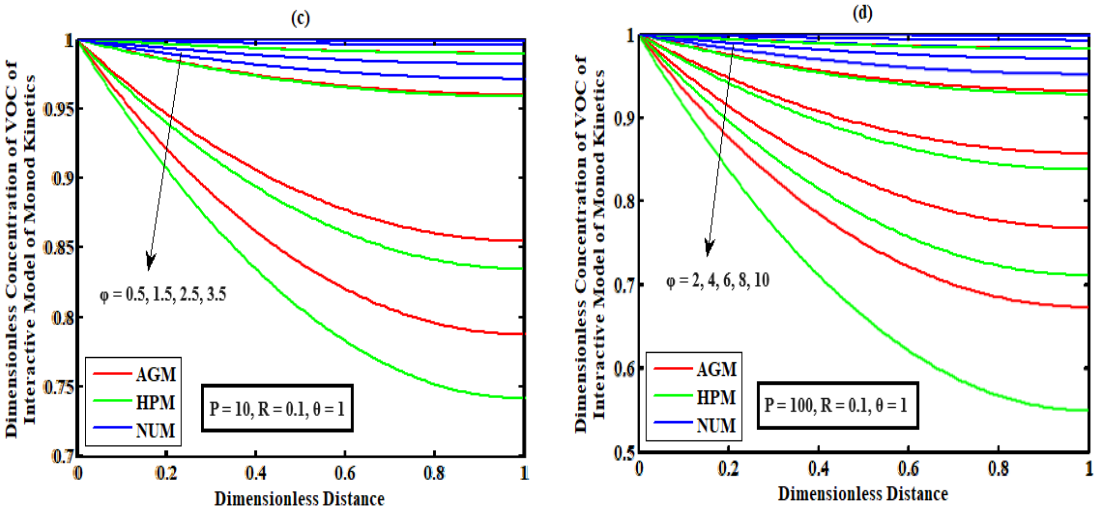

FIGURE 10. Plotting the dimensionless concentration $M(\chi)$ against the dimensionless distance χ for different Thiele moduli ϕ, P, R & θ values using equations (3.9) and (3.21)

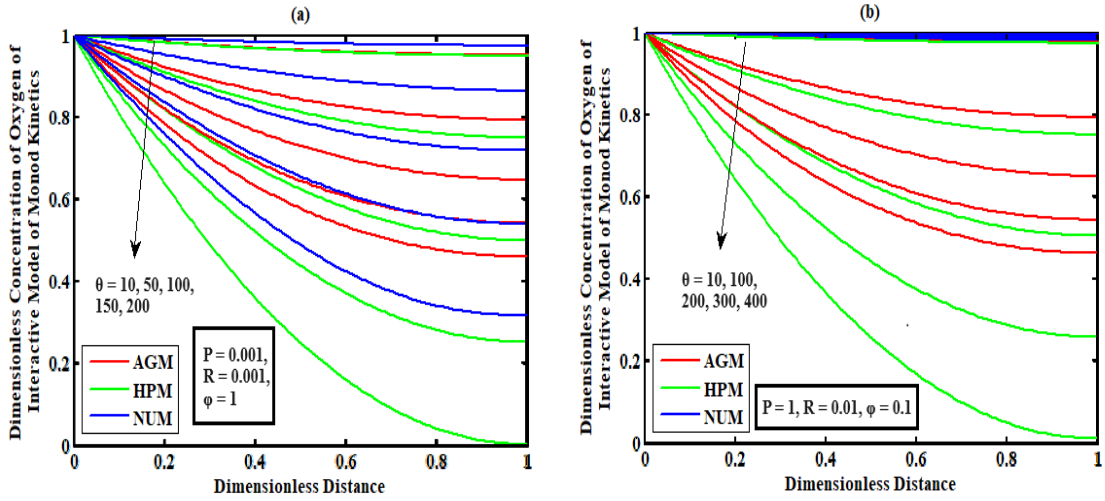

FIGURE 11. Plotting the dimensionless concentration $A(\chi)$ against the dimensionless distance χ for different Thiele moduli ϕ, P, R & θ values using equations (3.11) and (3.22)

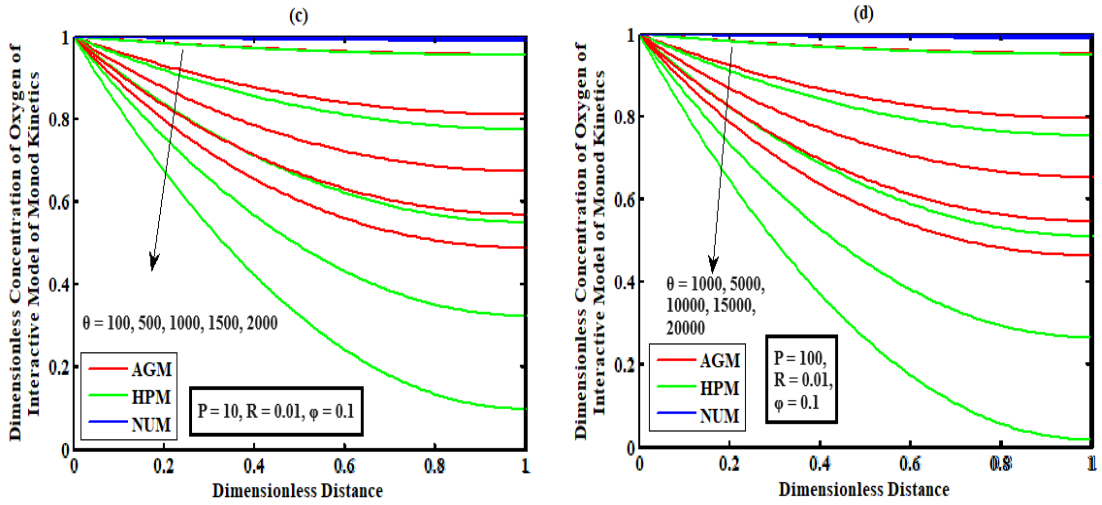

FIGURE 12. Plotting the dimensionless concentration $A(\chi)$ against the dimensionless distance χ for different Thiele moduli ϕ, P, R & θ values using equations (3.11) and (3.22)

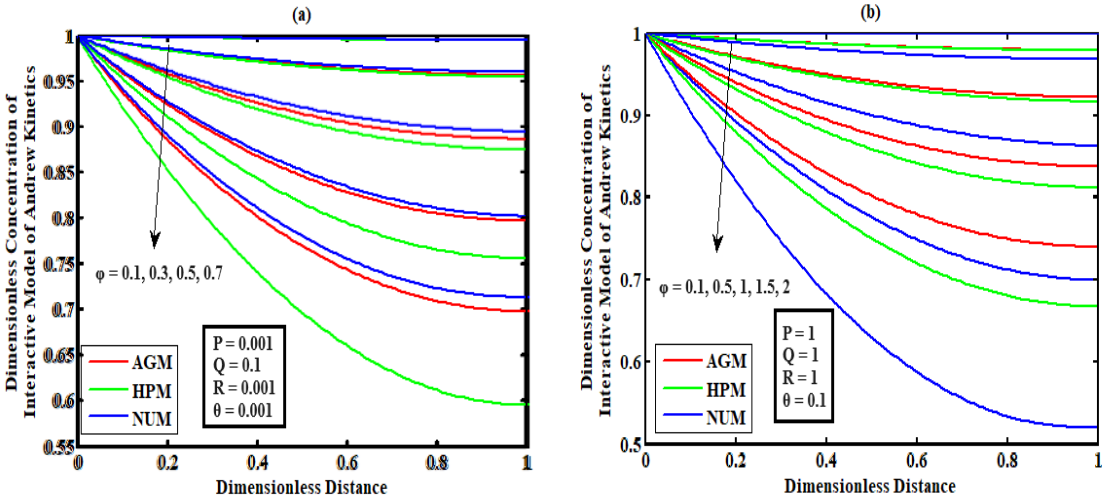

FIGURE 13. Plotting the dimensionless concentration $M(\chi)$ against the dimensionless distance χ for different Thiele moduli ϕ, P, Q, R & θ values using equations (3.13) and (3.23)

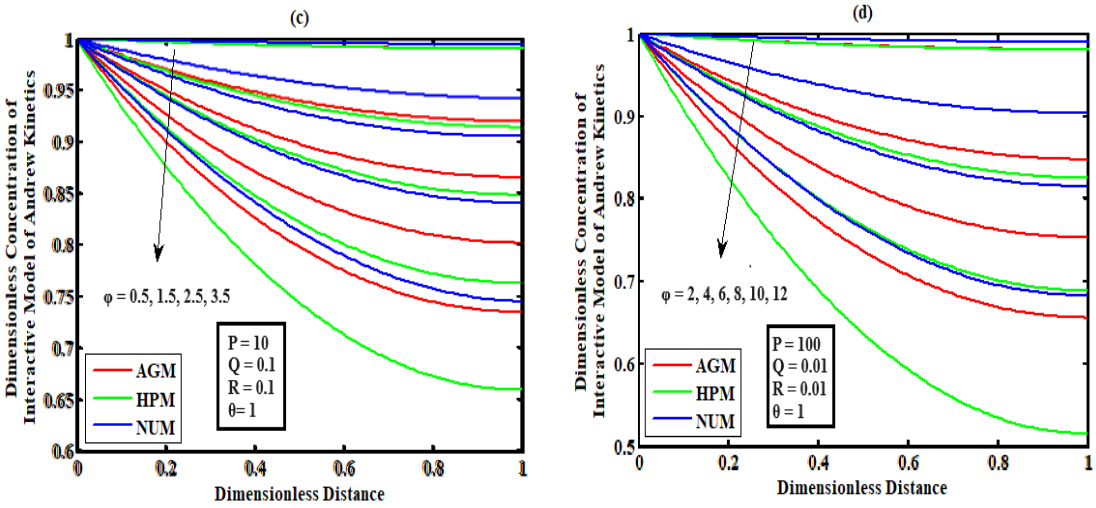

FIGURE 14. Plotting the dimensionless concentration $M(\chi)$ against the dimensionless distance χ for different Thiele moduli ϕ, P, Q, R & θ values using equations (3.13) and (3.23)

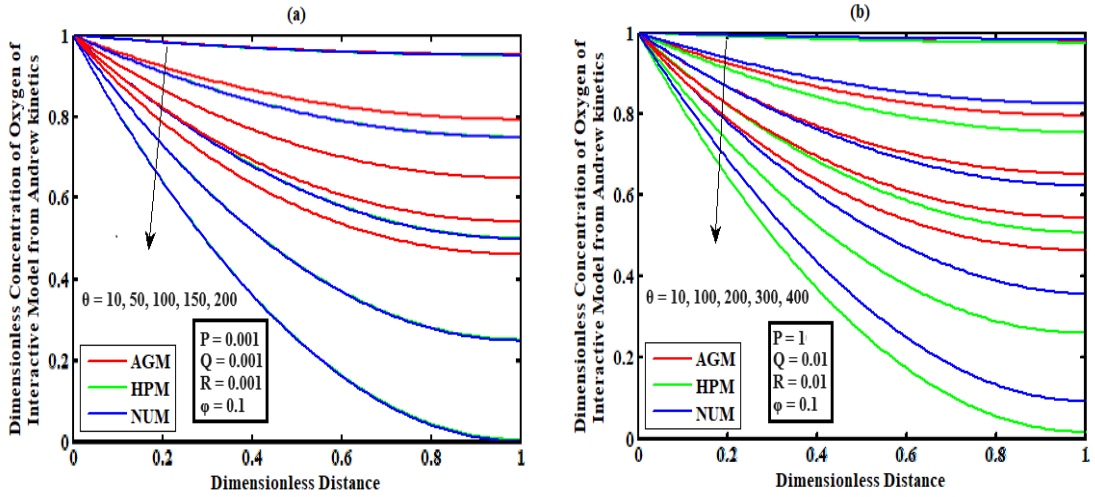

FIGURE 15. Plotting the dimensionless concentration $A(\chi)$ against the dimensionless distance χ for different Thiele moduli ϕ, P, Q, R & θ values using equations (3.15) and (3.24)

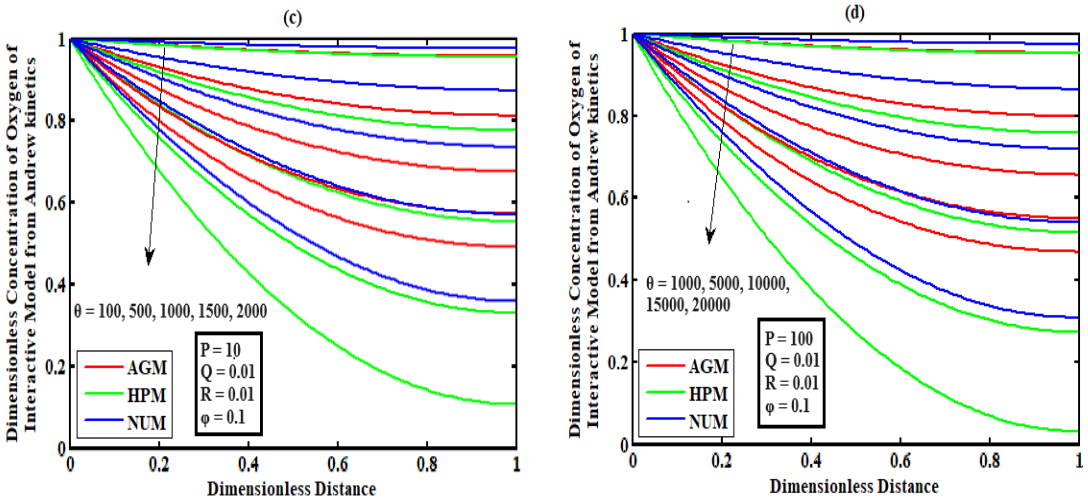

FIGURE 16. Plotting the dimensionless concentration $A(\chi)$ against the dimensionless distance χ for different Thiele moduli ϕ, P, Q, R & θ values using equations (3.15) and (3.24)

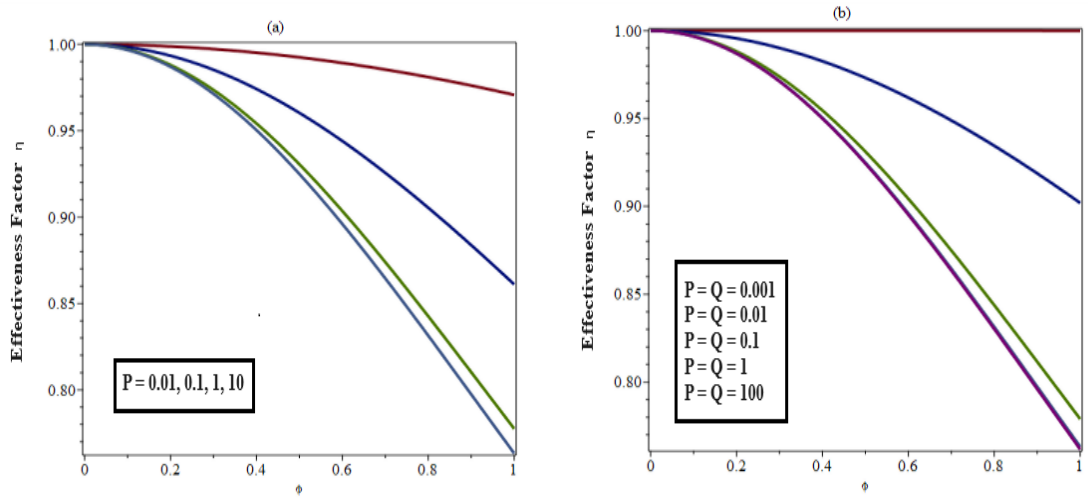

FIGURE 17. Effectiveness factor η against the Thiele modulus ϕ using the Equations (4.1) & (4.2)

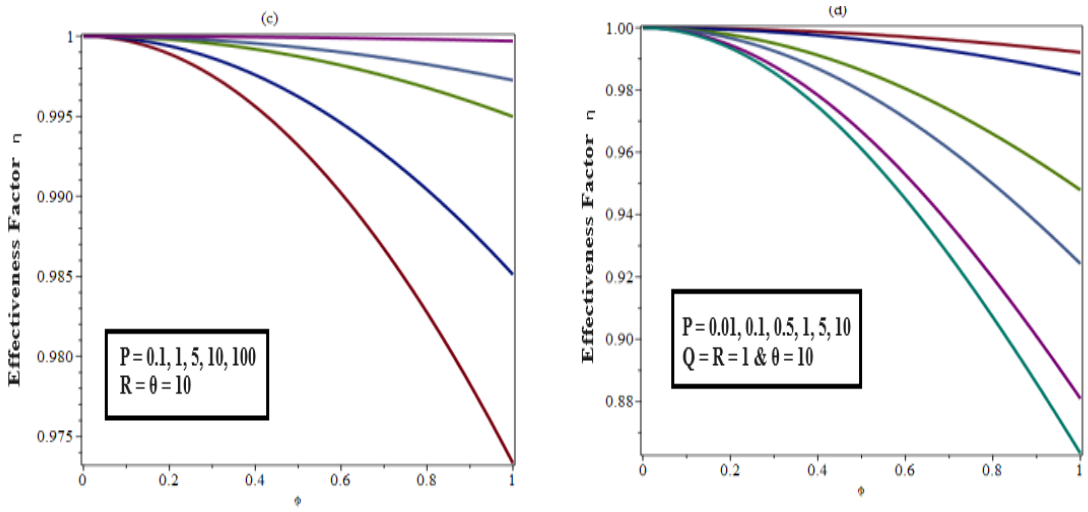

FIGURE 18. Effectiveness factor η against the Thiele modulus ϕ using the Equations (4.3) & (4.4)

NOMENCLATURE		
Symobols	Definitions	Units
m_h	Concentration of VOC in the gas phase at a height, h, along the column.	kg * m-3
m_{h_1}	Concentration of oxygen in the gas phase at a height, h, along the column.	kg * m-3
L_0	Kinetic constant	kg * m-3
L_1	Kinetic constant	kg * m-3
L_2	Kinetic constant	kg * m-3
U	Biofilm density defined as the dry weight of cell per volume of biofilm	kg * m-3
V	Amount of biomass produced per amount of VOC consumed	kg * kg-1
V_1	Amount of biomass produced per amount of oxygen consumed	kg * kg-1
D_1	Effective diffusion coefficient of VOC in the biofilm	m2 * s-1
D_2	Effective diffusion coefficient of oxygen in the biofilm	m2 * s-1
χ	Distance in the biofilm	m
β	Active biofilm thickness	m
β^2	Active biofilm thickness	m
λ	Specific growth rate of the biomass on VOC	h-1
λ_m	Maximum specific growth rate	h-1
λ^*	Kinetic constant	h-1
K	Air/biofilm distribution coefficient for the VOC as dictated by Henry's law	No unit
K_1	Air/biofilm distribution coefficient for the oxygen as dictated by Henry's law	No unit
$M(\chi)$	Dimensionless position in the bio layer concentration of VOC	No unit
$A(\chi)$	Dimensionless position in the bio layer concentration of oxygen	No unit
P	Dimensionless quantity	No unit
Q	Dimensionless quantity	No unit
R	Dimensionless quantity	No unit
θ	Dimensionless quantity	No unit
η	Effectiveness factor	No unit
ϕ^2	Square of Thiele modulus based on methanol	No unit

APPENDIX A

Apply the approximate analytical solutions for Equations (2.10) and (2.11) using the AGM technique, keeping in mind the boundary conditions (2.18) and (2.19). Make the relevant modifications as needed

$$M(\chi) = A_1 cosh(m\chi) + B_1 sinh(m\chi) \tag{7.1}$$

$$A(\chi) = A_2 cosh(n\chi) + B_2 sinh(n\chi) \tag{7.2}$$

where

$$A_1 = 1, B_1 = \frac{-sinh(m)}{cosh(m)}, A_2 = 1, B_2 = \frac{-sinh(m)}{cosh(m)} \tag{7.3}$$

Substitute equation (7.3) in (7.1) & (7.2), we obtain

$$m = \frac{\phi}{\sqrt{P+1}} \quad \& \quad n = \frac{\sqrt{(P+1)\theta}\phi}{P+1} \tag{7.4}$$

sub. Eqn (7.4) in Eqns. (2.10) & (2.11), we get

$$M(\chi) = cosh(m\chi) - \frac{sinh(m)sinh(m\chi)}{cosh(m)} \tag{7.5}$$

$$A(\chi) = cosh(n\chi) - \frac{sinh(n)sinh(n\chi)}{cosh(n)} \tag{7.6}$$

Equations (3.1) and (3.3) are obtained by replacing Equations (2.10) and (2.11) with Equations (7.5) and (7.6), respectively, and setting $\chi = 0$. We derive Equations (2.12) and (2.13), (2.14) and (2.15), and lastly (2.16) and (2.17), via this iterative approach. Make any necessary adjustments.

APPENDIX B

After implementing the HPM method, take into account the boundary conditions (2.18) & (2.19) and evaluate the approximate analytical solutions for Equations (2.10) and (2.11).

$$(1-p)\left(\frac{d^2M(\chi)}{d\chi^2}\right) + p\left(\frac{d^2M(\chi)}{d\chi^2} - \phi^2\left[\frac{M(\chi)}{1+PM(\chi)}\right]\right) = 0 \tag{7.7}$$

$$(1-p)\left(\frac{d^2A(\chi)}{d\chi^2}\right) + p\left(\frac{d^2A(\chi)}{d\chi^2} - \phi^2\theta\left[\frac{M(\chi)}{1+PM(\chi)}\right]\right) = 0 \tag{7.8}$$

Presented next is an approximate solution for Equation (7.7):

$$M(\chi) = M_0 + pM_1 + p^2M_2 + p^3M_3 + ... \tag{7.9}$$

We can obtain the following differential equation by replacing Equation (7.9) and comparing the coefficient of p^0.

$$p^0 : \frac{d^2M_0(\chi)}{d\chi^2} = 1 \tag{7.10}$$

$$p^1 : \frac{d^2M_1(\chi)}{d\chi^2} - \phi^2 \left[\frac{M_0(\chi)}{1 + PM_0(\chi)} \right] = 0 \tag{7.11}$$

The final equation (3.17) can be obtained by solving equations (7.10) and (7.11), providing that the boundary conditions specified in equations (2.18) and (2.19) are satisfied.

Conflicts of Interest: The authors declare that there are no conflicts of interest regarding the publication of this paper.

References

[1] L. Rajendran, R. Swaminathan, M. Chitra Devi, A Closer Look of Nonlinear Reaction-Diffusion Equations, Nova Science Publishers, New York, 2020.

[2] M.A. Deshusses, I.J. Dunn, Modeling Experiments on the Kinetics of Mixed-Solvent Removal from Waste Gas in a Biofilter, in: Proceedings of the 6th European Congress on Biotechnology, 1191–1198, Elsevier, 1994.

[3] K. Ranjani, R. Swaminathan, S.G. Karpagavalli, Mathematical Modelling of a Mono-Enzyme Dual Amperometric Biosensor for Enzyme-Catalyzed Reactions Using Homotopy Analysis and Akbari-Ganji Methods, Int. J. Electrochem. Sci. 18 (2023), 100220. https://doi.org/10.1016/j.ijoes.2023.100220.

[4] D.S. Hodge, J.S. Devinny, Modeling Removal of Air Contaminants by Biofiltration, J. Environ. Eng. 121 (1995), 21–32. https://doi.org/10.1061/(asce)0733-9372(1995)121:1(21).

[5] K. Ranjani, R. Swaminathan, SG. Karpagavalli, A Theoretical Investigation of Steady-State Concentration Processes at a Carrier-Mediated Transport Model Using Akbari-Ganji and Differential Transform Methods, Part. Diff. Equ. Appl. Math. 8 (2023), 100594. https://doi.org/10.1016/j.padiff.2023.100594.

[6] S.M. Zarook, A.A. Shaikh, Analysis and Comparison of Biofilter Models, Chem. Eng. J. 65 (1997), 55–61. https://doi.org/10.1016/s1385-8947(96)03101-4.

[7] J.H. He, Approximate Analytical Solution for Seepage Flow With Fractional Derivatives in Porous Media, Comp. Meth. Appl. Mech. Eng. 167 (1998), 57–68. https://doi.org/10.1016/s0045-7825(98)00108-x.

[8] A. Reena, SG. Karpagavalli, L. Rajendran, B. Manimegalai, R. Swaminathan, Theoretical Analysis of Putrescine Enzymatic Biosensor With Optical Oxygen Transducer in Sensitive Layer Using Akbari–ganji Method, Int. J. Electrochem. Sci. 18 (2023), 100113. https://doi.org/10.1016/j.ijoes.2023.100113.

[9] J.H. He, Homotopy Perturbation Method for Solving Boundary Value Problems, Phys. Lett. A 350 (2006), 87–88. https://doi.org/10.1016/j.physleta.2005.10.005.

[10] A. Reena, SG. Karpagavalli, R. Swaminathan, Theoretical Analysis and Steady-State Responses of the Multienzyme Amperometric Biosensor System for Nonlinear Reaction-Diffusion Equations, Int. J. Electrochem. Sci. 18 (2023), 100293. https://doi.org/10.1016/j.ijoes.2023.100293.

[11] B. Jang, Two-Point Boundary Value Problems by the Extended Adomian Decomposition Method, J. Comp. Appl. Math. 219 (2008), 253–262. https://doi.org/10.1016/j.cam.2007.07.036.

[12] A. Uma, R. Swaminathan, Mathematical Analysis of Nonlinear Reaction Diffusion Process at Carbon Dioxide Absorption in Concentrated Mixtures of 2-Amino-2-Methyl-1-Proponal and 1,8-Diamino-p-Methane, Int. J. Anal. Appl. 22 (2024), 110. https://doi.org/10.28924/2291-8639-22-2024-110.

[13] G. Adomian, Stochastic Nonlinear Modeling of Fluctuations in a Nuclear Reactor-A New Approach, Ann. Nuclear Energy 8 (1981), 329–330. https://doi.org/10.1016/0306-4549(81)90053-0.

[14] A. Soufyane, M. Boulmalf, Solution of Linear and Nonlinear Parabolic Equations by the Decomposition Method, Appl. Math. Comp. 162 (2005), 687–693. https://doi.org/10.1016/j.amc.2004.01.005.

[15] R. Raja, R. Swaminathan, Mathematical Analysis of Nonlinear Differential Equations in Polymer Coated Microelectrodes, Contemp. Math. 5 (2024), 2585–2598. https://doi.org/10.37256/cm.5220244426.

[16] M. Sivasankari, L. Rajendran, Analytical Expressions of Concentration of VOC and Oxygen in Steady-State in Biofilteration Model, Appl. Math. 04 (2013), 314–325. https://doi.org/10.4236/am.2013.42048.

[17] A. Nebiyal, R. Swaminathan, SG. Karpagavalli, Reaction Kinetics of Amperometric Enzyme Electrode in Various Geometries Using the Akbari-Ganji Method, Int. J. Electrochem. Sci. 18 (2023), 100240. https://doi.org/10.1016/j.ijoes.2023.100240.

[18] K. Ranjani, R. Swaminathan, SG. Karpagavalli, Mathematical Modelling of Three-Layer Amperometric Biosensor and Analytical Expressions Using Homotopy Perturbation Method, Part. Diff. Equ. Appl. Math. 11 (2024), 100755. https://doi.org/10.1016/j.padiff.2024.100755.

[19] R. Swaminathan, K.L. Narayanan, V. Mohan, K. Saranya, L. Rajendran, Reaction/Diffusion Equation with Michaelis-Menten Kinetics in Microdisk Biosensor: Homotopy Perturbation Method Approach, Int. J. Electrochem. Sci. 14 (2019), 3777–3791. https://doi.org/10.20964/2019.04.13.

[20] A. Reena, R. Swaminathan, Mathematical Investigation of Non-Linear Reaction-Diffusion Equations on Multiphase Flow Transport in the Entrapped-Cell Photobioreactor Using Asymptotic Methods, Int. J. Anal. Appl. 22 (2024), 74. https://doi.org/10.28924/2291-8639-22-2024-74.

[21] A. Uma, R. Raja, R. Swaminathan, Analytical Solution of Concentrated Mixtures of Hydrogen Sulfide and Methanol in Steady State in Biofilm Model, Contemp. Math. 5 (2024), 2632–2645. https://doi.org/10.37256/cm.5320244394.